FEBS Letters 581 (2007) 2416–2422

Crystal structures of catrocollastatin/VAP2B reveal a dynamic, modular architecture of ADAM/adamalysin/reprolysin family proteins

Tomoko Igarashi[a], Satohiko Araki[b], Hidezo Mori[a], Soichi Takeda[a,*]

[a] *Department of Cardiac Physiology, National Cardiovascular Center Research Institute 5-7-1 Fujishiro-dai, Suita, Osaka 565-8565, Japan*
[b] *Sugashima Marine Biological Laboratory, Graduate School of Science, Nagoya University, Toba, Mie 517-0004, Japan*

Received 26 January 2007; revised 29 March 2007; accepted 20 April 2007

Available online 30 April 2007

Edited by Christian Griesinger

Abstract Catrocollastatin/vascular apoptosis-inducing protein (VAP)2B is a metalloproteinase from *Crotalus atrox* venom, possessing metalloproteinase/disintegrin/cysteine-rich (MDC) domains that bear the typical domain architecture of a disintegrin and metalloproteinase (ADAM)/adamalysin/reprolysin family proteins. Here we describe crystal structures of catrocollastatin/VAP2B in three different crystal forms, representing the first reported crystal structures of a member of the monomeric class of this family of proteins. The overall structures show good agreement with both monomers of atypical homodimeric VAP1. Comparison of the six catrocollastatin/VAP2B monomer structures and the structures of VAP1 reveals a dynamic, modular architecture that may be important for the functions of ADAM/adamalysin/reprolysin family proteins.

Keywords: ADAM; Adamalysin; Reprolysin; MDC protein; Metalloproteinase disintegrin; Apoptotic toxin

1. Introduction

Hemorrhagic snake venoms induce local and systemic hemorrhaging by disrupting the walls of the blood vessels in envenomed patients [1]. In vitro, they induce apoptosis specifically in cultured vascular endothelial cells [2]. Vascular apoptosis-inducing protein (VAP)1 and VAP2 were originally isolated from *Crotalus atrox* venom [3,4], and similar apoptotic toxins have been isolated from other snake venoms [5–7]. VAP1 is a disulfide-bridged homodimeric protein with an apparent molecular weight of 110 kDa, and an isoelectric point of 8.5. VAP2 is a single chain protein with a MW of 55 kDa and an isoelectric point of 4.5 [3,4,8]. VAPs are members of the P-III class of snake venom metalloproteinases (SVMPs), possessing a metalloproteinase/disintegrin/cysteine-rich (MDC) domain architecture typical of a disintegrin and metalloproteinase (ADAM)/adamalysin/reprolysin family proteins [9,10]. VAP-induced apoptosis is dependent on its catalytic activity [8], is inhibited by antibodies to integrins α3, α6, β1 and CD9 [11], and involves activation of specific caspases [12]. However, the physiological targets of VAPs and the underlying mechanism of VAP-induced apoptosis remain elusive.

ADAMs are a family of mammalian membrane-anchored glycoproteins that have been implicated in the processing of cell surface and extracellular matrix proteins [13,14]. The crystal structures of several P-I class SVMPs, which contain only a metalloproteinase (M)-domain, and the isolated M and disintegrin/cysteine-rich (DC) domains of ADAMs have been determined [15–18]. However, structures of ADAM/adamalysin/reprolysin family proteins that include the entire MDC domain have not been determined. The relevance of the multidomain structure to the catalytic and adhesive functions of this family of proteins is an important issue that remains to be elucidated. To better understand the structure–function relationship of ADAM/adamalysin/reprolysin family proteins, and how it relates to the molecular mechanism of VAP-induced apoptosis, we have been engaged in crystallographic studies of VAPs. Recently, we determined the crystal structure of VAP1, revealing the MDC domain architecture for the first time [19]. Although the intrinsic two-fold symmetry of atypical homodimeric VAP1 conferred a great advantage for both its crystallization and structural resolution, the possibility remained that the spatial arrangement of the MDC domains of VAP1 differed from that of monomeric SVMPs and ADAMs, due to crystallographic restraints imposed on the molecule. The majority of ADAMs and SVMPs do not to form VAP1-type dimers, most likely due to the lack of a consensus QDHSK sequence [19] (residues 320–324 in VAP1, in which the Nζ atom of Lys324 is coordinated by the six oxygen atoms of another monomer and plays a pivotal role in dimer formation), and Cys365, which are conserved among the dimeric SVMPs (Supplementary Fig. 1). Therefore, to elucidate the general architecture of proteins of the ADAM/adamalysin/reprolysin family, we crystallized VAP2 and determined its structure. We modeled all of the structures as monomers of VAP2B, which is identical to catrocollastatin, a protein previously isolated as a platelet aggregation inhibitor [20]. Here we describe the structure of catrocollastain/VAP2B, as determined in three different crystal forms. These are the first reported crystal structures of the monomeric class of proteins in ADAM/adamalysin/reprolysin family.

2. Materials and methods

Protein preparation and crystallization were performed as previously described [21]. The diffraction data sets were collected at the

*Corresponding author. Fax: +81 6 6872 7485.
E-mail address: stakeda@ri.ncvc.go.jp (S. Takeda).

Abbreviations: ADAM, a disintegrin and metalloproteinase; MDC, Metalloproteinase/disintegrin/cysteine-rich; SVMP, Snake venom metalloproteinase; HVR, Hyper-variable-region; ncs, Non-crystallographic symmetry; VAP, Vascular apoptosis-inducing protein; PEG, Polyethyleneglycol

0014-5793/$32.00
doi:10.1016/j.febslet.2007.04.057

SPring-8 beamline BL41XU using the ADSC quantum 315 CCD detector with a wavelength of 1.0 Å at 100 K. Images were reduced using HKL2000 [22] (Table 1). Structures were solved using the molecular replacement (MR) method and the MOLREP program of the CCP4 suite [23], with the structure of VAP1 (2ERO) as a starting model. The M- and C-domains of the VAP1 were used separately as the search models. An MR solution was initially obtained from the Form 2-2 crystal data set, which assumed two M-domains and two C-domains in the asymmetric units. After the model was manually rebuilt using TURBO-FRODO [24], it was subjected to torsional molecular dynamic refinements using CNS [25]. Iterative refinements and manual rebuilding of the model improved the electron-density map and enabled us to model the remaining part of the molecule. The composite omit electron-density maps created by CNS were used to confirm the chain tracing. After the polypeptide chains were modeled, we modeled zinc and calcium ions and the inhibitor GM6001 (3-(*N*-hydroxycarboxamide)-2-isobutyl-propanoyl-Trp-methylamide), then the components of the carbohydrate chain linked to Asn371.

The two monoclinic crystal structures were solved by MR with the domains of the refined Form 2-2 crystal structure as a starting model. In all three crystal forms, the asymmetric unit contained two monomers of catrocollastatin/VAP2B. Refinement statistics are shown in Table 1. During the course of our analysis, we found a point mutation (F203V) in the crystallized specimens. By comparing the structures with that of VAP1, which has a phenylalanine at this position, we determined that this mutation does not introduce a large structural change or affect the flexibility of the molecule. Graphical representations were prepared using the programs TURBO-FRODO [24], MOLSCRIPT [26], RASTER3D [27] and PyMOL [28].

3. Results and discussion

3.1. Structural determination

Purified VAP2 was crystallized in variety of forms [21]. In the current study, we determined the structures of three of these crystal forms. Previously, we observed that the VAP2 preparation is a mixture of two homologous polypeptide chains, VAP2A and VAP2B [29]. To identify the molecules in the crystals as either VAP2A or catrocollastatin/VAP2B, we carefully analyzed the composite omit electron-density maps corresponding to the 11 amino acid residues that are distinct between the two proteins (Supplementary Fig. 1). Based on this assessment, the major component in the three crystals was determined to be catrocollastain/VAP2B. Therefore, in the present study, we modeled all six molecules as catrocollastain/VAP2B. The indole ring of GM6001 provided additional

Table 1
Data collection and refinement statistics

	Form 2-1	Form 2-2	Form 2-5
Data collection			
Space group	$P2_1$	$P2_12_12_1$	$C2$
Cell dimensions			
a, *b*, *c* (Å)	56.9, 138.0, 59.2	57.7, 118.2, 138.5	220.7, 79.5, 58.7
α, β, γ (°)	90, 91.5, 90	90, 90, 90	90, 91.7, 90
Resolution (Å) (high resolution shell)	50–2.15(2.23–2.15)	50–2.50(2.59–2.50)	50–2.70(2.80–2.70)
No. of unique reflections	48664(4428)	33288(2925)	26911(2313)
[a] R_{merge}	0.081(0.196)	0.089(0.321)	0.085(0.231)
$I/\sigma(I)$	9.8(4.6)	10.3(3.7)	10.1(5.5)
Completeness (%)	98.1(89.5)	98.6(88.4)	95.9(82.5)
Redundancy	3.3(2.0)	6.5(3.3)	3.4(2.8)
Refinement			
Resolution (Å) (high resolution shell)	50–2.15(2.23–2.15)	50–2.50(2.59–2.50)	50–2.70(2.80–2.70)
No. of reflections	48628(4386)	33099(2922)	26907(2276)
[b] R_{work}	0.175(0.195)	0.227(0.316)	0.199(0.264)
[c] R_{free}	0.228(0.277)	0.286(0.399)	0.260(0.328)
Average B-factors (No. of atoms)			
All atoms	19.9(7292)	38.5(6801)	25.1(6823)
Protein	18.5(6422)	38.1(6438)	24.7(6438)
Main chain atoms	17.2	36.9	23.1
Side chain atoms	19.9	39.5	26.5
Zn^{2+}	13.6(2)	24.9(2)	18.7(2)
Ca^{2+}	14.6(6)	41.4(6)	21.5(6)
Carbohydrate	54.2(139)	81.4(88)	37.4(226)
GM6001	16.2(56)	36.9(56)	0(-)
Water	26.5(668)	31.6(211)	22.2(151)
R.m.s deviations			
Bond lengths (Å)	0.0047	0.0065	0.0045
Bond angles (°)	1.20	1.44	1.14
Ramachandran plot			
Most favored	87.2%	84.3%	82.8%
Additional allowed	12.1%	15.0%	16.4%
Generously allowed	0.4%	0.6%	0.4%
Disallowed	0.1%(R297B)	0.1%(R297B)	0.3%(R297A/R297B)

[a] $R_{merge} = \Sigma_{hkl}\Sigma_i \mid I_i(hkl) - \langle I(hlk)\rangle|/\Sigma_{hkl}\Sigma_i I_i(hkl)$, where $I_i(hkl)$ is the *i*th intensity measurement of reflection *hkl* and $\langle I(hlk)\rangle$ is its average.
[b] $R_{work} = \sum\|F_{obs}| - |F_{calc}\|/\sum|F_{obs}|$.
[c] R_{free} = *R*-value for a randomly selected subset (5%) of the data that were not used for minimization of the crystallographic residual. A single crystal was used for measurement of each data set.

crystal contacts for the neighboring molecule, resulting in crystals that were distinct from the inhibitor-free form.

3.2. Overall structure

The overall structure of catrocollastatin/VAP2B is presented in Fig. 1. The structure of the M-domain was very similar to the corresponding structures in adamalysin II [15] and ADAM33 [17], with a flat elliptical shape and a core formed by a five-stranded β-sheet and four α-helices. A conserved methionine (Met357, Met-turn) was present downstream of the consensus HEXXHXXGXXHD sequence, which contains three histidines (His333, His337 and His343) that function as ligands of the catalytic zinc atom, and a glutamate residue (Glu334) that functions as the general base (Fig. 2). These structural features are typical of the metzincine family of metalloproteinases [30,31]. A bound calcium ion was identified opposite the active site cleft and close to the crossover point of the N- and C-terminal segments of the M-domain (Ca^{2+}-binding site I), as in the structures of adamalysin II [15] and ADAM33 [17]. The M-domain is followed by the D-domain, which can be sub-divided into "shoulder" (D_s) and "arm" (D_a) segments. D_s protrudes from the M-domain close to Ca^{2+}-binding site I, opposing the catalytic zinc atom. The C-domain is sub-divided into "wrist" (C_w) and "hand" (C_h) segments. Because of its curved structure, with the concave surface toward the M-domain, the distal portion of C_h comes close to and faces the catalytic site, thus the entire molecule adopts a C-shaped conformation. In the D_s and D_a segments, there are Ca^{2+} ions (sites II and III, respectively) that stabilize the structure. Details of the Ca^{2+}-coordinations are shown in Supplementary Fig. 2. The distal portion of the C-shape, spanning residues 561–582 of the C_h domain, is the region in which the amino acid sequence is most divergent and variable in length among ADAM/adamalysin/reprolysin family proteins (Fig. 2 and Supplementary Fig. 1). We designated this region as the hyper-variable-region (HVR), and have proposed that it represents a potential exosite for target recognition [19]. Aside from Cys377, whose side chain is embedded in the hydrophobic core, all 34 cysteinyl residues are involved in disulfide bonding. The number and spacing of cysteinyl residues, and the structures of the Ca^{2+}-binding sites are strictly conserved among ADAM/adamalysin/reprolysin family proteins (Fig. 2 and Supplementary Fig. 1). Fig. 2 shows the sequence alignment of a selected subset of ADAMs and SVMPs; alignment of the full sequences of catrocollastatin/VAP2B and 107 proteins of the ADAM/adamalysin/reprolysin family can be found in Supplementary Fig. 1.

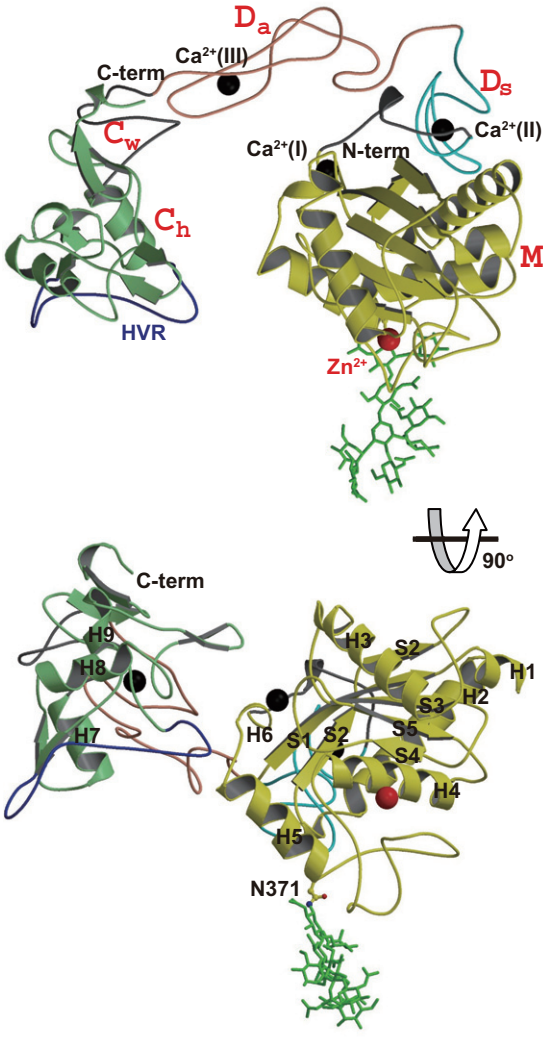

Fig. 1. Ribbon diagrams of catrocollastatin/VAP2B. The M-domain, linker, D_s, D_a, C_w, and C_h segments and the HVRs are shown in red, yellow, grey, cyan, pink, grey, green and blue, respectively. Zinc and calcium ions are represented as red and black spheres, respectively. The carbohydrate moiety linked to Asn371 is shown as a stick representation.

3.3. Flexible modular architecture

The structures of the M-domain (Fig. 3A), D_s (Fig. 3C), and C_w/C_h (Fig. 3B) of the six catrocollastatin/VAP2B molecules were nearly identical (r.m.s.d of 0.33, 0.45 and 0.59 Å, respectively). They were also essentially the same as the corresponding regions of VAP1 (r.m.s.d of 0.78, 0.63 and 1.1 Å, respectively (Fig. 3A–C)). However, the relative orientations of the sub-domains were quite variable. The largest difference was observed when the M domains of the six catrocollastatin/VAP2B molecules are superimposed. The $D_s/D_a/C_w/C_h$ portion should be rotated by approximately 13° relative to the M-domain, bringing about a 15-Å displacement at the distal end of C_h (Fig. 3A). A similar plot of the C_h segments superimposed shows less hinge bending, bringing approximately a 6-Å displacement at the distal portion of D_s (Fig. 3B). This conformed that the hinge motion occurs largely between the M domain and D_s. The bending of the main chain at two residues, Val403 and Gly438, is most prominent (Fig. 3C), however, the entire linker region (which is defined by the segment between two structural Ca^{2+}-binding sites, I and II) also moves in concert with the bending motion of Val403 (Fig. 3D). In this concerted movement of the linker, the side chain of Leu408 in D_s is positioned at a pivotal point (Fig. 3D and E). The main chain carbonyl oxygen atom of Leu408 coordinates the calcium ion at site II, whereas, the side-chain of Leu408 protrudes from D_s and interacts with a small hydrophobic cavity on the surface of the M domain (Fig. 3D). A balky hydrophobic residue (Leu or Phe or Tyr) at this position is highly conserved among ADAM/adamalysin/reprolysin family proteins (Supplementary Fig. 1), and its side chain probably functions as

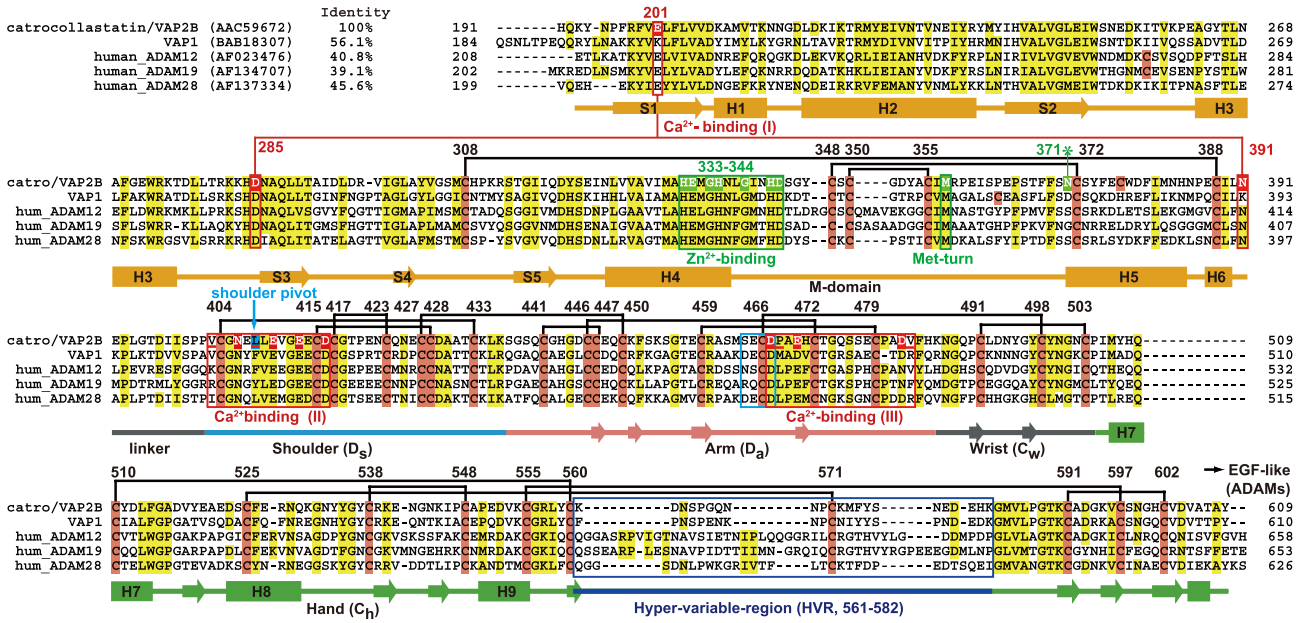

Fig. 2. Sequence alignment of catrocollastatin/VAP2B, VAP1 and human ADAMs. The cysteinyl residues and the conserved residues are shaded in pink and yellow, respectively. Disulfide bridges, secondary structures and domains are drawn schematically. The HVR, Ca^{2+}-binding sites, Zn^{2+}-binding site and disintegrin-loop are boxed in blue, red, green and cyan, respectively. The Ca^{2+}-coordinating residues are shaded in red.

a universal joint (shoulder joint) that allows D_s to adopt various orientations with respect to the M domain. The linker has fewer specific interactions with D_s and has a rather high B-factor (Supplementary Figs. 3 and 4). It is divergent and variable in length (7–12 aa), particularly in human ADAMs (Supplementary Fig. 1), thus may function primarily in connecting D_s to the M domain. The linker may also restrict the mobility of the shoulder joint, and thus determine the preferred orientation of the M domain of each ADAMs relative to the rest of the molecule for distinct targets. The residues forming the hydrophobic cavity with which Leu408 interacts are less conserved and also have relatively high B-factors (Supplementary Figs. 3 and 4). Thus they may also contribute to the flexibility of the shoulder joint.

Previously, we suggested a putative mechanism of HVR-mediated target recognition and catalysis by this family of proteins [19]. The present study allows us to incorporate into the previous model that intrinsic flexibility may be important for fine-tuning substrate recognition, by adjusting the spatial alignment of the catalytic and adhesion sites during the catalytic cycle (Fig. 3F). The structure of the lower half of the D_a segment in catrocollastatin/VAP2B was different from that of VAP1 (Fig. 3B and Supplementary Fig. 3C), most likely due to the substitution of Glu470 (in catrocollastatin/VAP2B) with Asp471 (in VAP1), and the insertion of Pro480 (in catrocollastatin/VAP2B). All the ADAMs, with the exception of ADAMs 10 and 17, which lack Ca^{2+}-binding site III, and the monomeric P-III and P-IV SVMPs contain Glu470 and Pro480 (see Supplementary Fig. 1). Thus, it is likely that they adopt a more catrocollastatin/VAP2B-like structure. As was observed in VAP1, the disintegrin-loop is packed by C_w, and forms a less flexible D_a/C_w junction, and therefore is unavailable for ligand binding. Differences in the orientation of D_a and C_w among these proteins may be important for proper spatial alignment of the catalytic and adhesion units and for substrate binding specificity. The angle between C_w and C_h in catrocollastatin/VAP2B was nearly invariant. It was essentially the same as that seen in VAP1 (Fig. 3B), but substantially different than that of ADAM10 [18,19]. Whether different ADAM/adamalysin/reprolysin family proteins have distinct C_w/C_h orientations remains to be established.

3.4. Modular architecture and post-translational processing

The disintegrins that are commonly found in Viperid venoms are typically generated by proteolytic processing of larger precursor molecules, the P-II class of SVMPs, which contain an M-domain plus a disintegrin portion [32,33]. The flexible modular structure described above points to a potential mechanism of selection of cleavage sites for this processing event. The cleavage sites of the medium-sized disintegrins (~70 amino acids) are usually within Ca^{2+}-binding site II, whereas, those of the shorter ones (41–51 residues) are at the boundary between D_s and D_a. The longer disintegrins (~84 residues) are processed within the linker between M and D_s (Fig. 4 and Supplementary Fig. 1). Most of the P-II SVMPs have fewer cysteine residues within their D_s segment (3 or 5 cysteine residues, see Supplementary Fig. 1) compared to P-III SVMPs, and thus have fewer disulfide bonds. Additionally, they contain substitutions of the calcium-binding residues at site II, indicating that they have a less stable D_s structure compared to P-III SVMPs. Long disintegrins have the same number of cysteine residues (7 cysteine residues) and Ca^{2+}-binding residues at site II as P-III SVMPs and ADAMs, and thus would be predicted to have a more stable D_s structure, which may account for their cleavage at the linker between M and D_s. A protective role for calcium against auto proteolysis in the linker region has been reported [34], and the linker region is usually removed from P-I SVMPs post-translationally [35]. Collectively, these observations suggest that differential susceptibility to proteolysis in the linker region and D_s, due to variability in the number of disulfide bonds and the presence or absence of bound calcium at site II, may underlie the

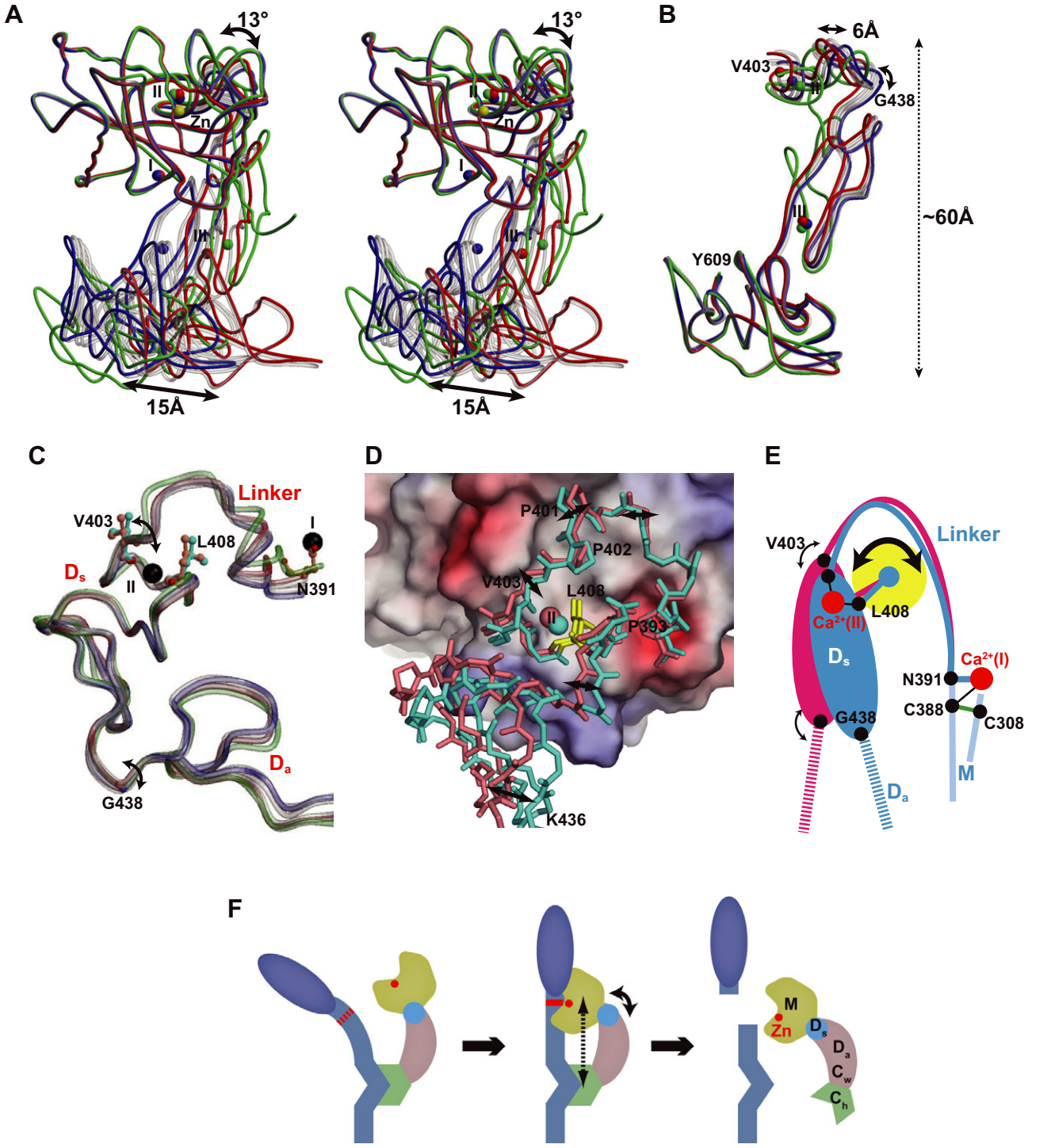

Fig. 3. Mobility of the sub-domains. (A) The M-domains of the six catrocollastatin/VAP2B molecules and the VAP1 monomer were superimposed and are shown in stereo. Two representative catrocollastatin/VAP2B molecules are shown in blue and red, the other four catrocollastatin/VAP2B molecules are in gray, and the VAP1 monomer is in green. The zinc ion is shown as a yellow sphere. The calcium atoms bound to the red and blue catrocollastatin/VAP2B molecule and VAP1 are shown as red, blue and green spheres, respectively. Superimposition of the D_h and C_s segments of the six catrocollastatin/VAP2B molecules and the VAP1 monomer are shown in B and C, respectively. (D) Close-up view of the shoulder joint. The molecular surface of the M-domain is colored according to the electrochemical surface potential (red to blue). The linker and part of the D_s segment of the two representative catrocollastatin/VAP2B molecules are shown as stick representations in pink and cyan, respectively. (E) Schematic diagram of the hinge motion at the shoulder joint. (F) Schematic model of substrate recognition and cleavage by a soluble ADAM/adamalysin/reprolysin protein.

generation of disintegrins with different lengths. Fertilin α (ADAM1) and β (ADAM2) undergo proteolytic processing within Ca^{2+}-binding site III and the linker region, respectively at different stages of sperm maturation (Fig. 4, Supplementary Fig. 1) [36,37]. The current structural data suggests that Ca^{2+}-binding, together with a flexible modular structure, may also

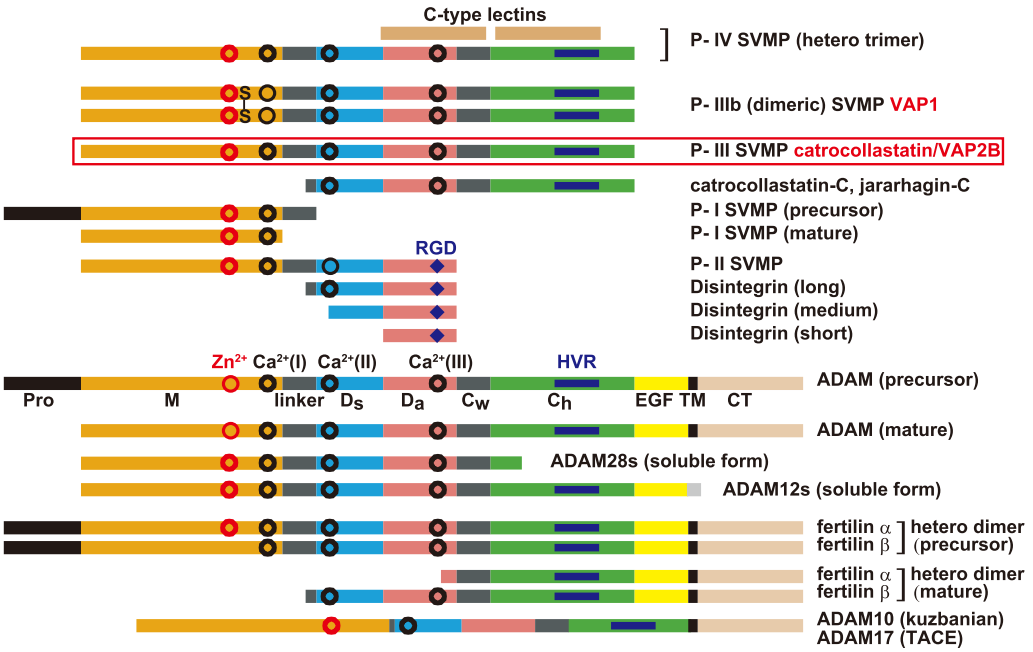

Fig. 4. Schematic representation of the modular architecture of ADAM/adamalysin/reprolysin family proteins. Each sub-domain is colored as for Fig. 1; the pro-domain (Pro), EGF-like domain (EGF), transmembrane region (TM) and cytoplasmic domain (CT) are in black, yellow, black and light salmon, respectively. The RGD sequences in disintegrins and an interchain disulfide bond in VAP1 are indicated. The Zn^{2+} and Ca^{2+} ions are shown as red and black circles, respectively; the closed circles indicate that all the members have a complete metal-binding sequence, whereas, open circles indicate that some members do not have it.

play a role in differential proteolytic processing of precursor proteins, giving rise to the biochemical and functional complexity of Crotalid and Viperid snake venoms, as well as post-translational regulation of ADAMs' functions.

4. Conclusion

ADAMs are widely distributed and constitute major membrane-bound sheddases that proteolytically process cell-surface-proteins for cell–cell communication. As such, they have emerged as potential therapeutic targets for a variety of diseases. SVMPs are key toxins involved in venom-induced pathogenesis, and thus are important targets for antivenom therapeutics. However, the physiological targets of ADAMs and SVMPs, and the molecular mechanism of target recognition are poorly understood. The structures presented here reveal a dynamic, modular architecture of the MDC domains of ADAM/adamalysin/reprolysin family proteins. Intrinsic flexibility may be important for fine-tuning substrate recognition, adjusting the spatial alignment of the catalytic and adhesion sites, and for post-translational regulation of this family of proteins.

Acknowledgement: We thank M. Tomisako for her help in crystallization experiments. This work was partly supported by Grant nano-001 for Research on Advanced Medical Technology from the Ministry of Health, Labor, and Welfare of Japan, and by grants from the Takeda Science Foundation, from the Kao Foundation for Arts and Science, from Mitsubishi Pharma Research Foundation and from Senri Life Science Foundation. T. I is supported by the grant from New Energy and Industrial Technology Development Organization (NEDO) of Japan.

Appendix A. Supplementary data

The atomic coordinates and structure factors have been deposited in the Protein Data Bank under accession codes 2DW0, 2DW1 and 2DW2 for the Form 2-1, Form 2-2 and Form 2-5 crystals, respectively. Supplementary data associated with this article can be found, in the online version, at doi:10.1016/j.febslet.2007.04.057.

References

[1] Gutierrez, J.M., Rucavado, A., Escalante, T. and Diaz, C. (2005) Hemorrhage induced by snake venom metalloproteinases: biochemical and biophysical mechanisms involved in microvessel damage. Toxicon 45, 997–1011.
[2] Araki, S., Ishida, T., Yamamoto, T., Kaji, K. and Hayashi, H. (1993) Induction of apoptosis by hemorrhagic snake venom in vascular endothelial cells. Biochem. Biophys. Res. Commun. 190, 148–153.
[3] Masuda, S., Araki, S., Yamamoto, T., Kaji, K. and Hayashi, H. (1997) Purification of a vascular apoptosis-inducing factor from hemorrhagic snake venom. Biochem. Biophys. Res. Commun. 235, 59–63.
[4] Masuda, S., Hayashi, H. and Araki, S. (1998) Two vascular apoptosis-inducing proteins from snake venom are members of the metalloprotease/disintegrin family. Eur. J. Biochem. 253, 36–41.
[5] Trummal, K. et al. (2005) A novel metalloprotease from Vipera lebetina venom induces human endothelial cell apoptosis. Toxicon 46, 46–61.
[6] Masuda, S., Hayashi, H., Atoda, H., Morita, T. and Araki, S. (2001) Purification, cDNA cloning and characterization of the vascular apoptosis-inducing protein, HV1, from Trimeresurus flavoviridis. Eur. J. Biochem. 268, 3339–3345.
[7] You, W.K., Seo, H.J., Chung, K.H. and Kim, D.S. (2003) A novel metalloprotease from Gloydius halys venom induces endothelial

cell apoptosis through its protease and disintegrin-like domains. J. Biochem. (Tokyo) 134, 739–749.
[8] Masuda, S., Ohta, T., Kaji, K., Fox, J.W., Hayashi, H. and Araki, S. (2000) cDNA cloning and characterization of vascular apoptosis-inducing protein 1. Biochem. Biophys. Res. Commun. 278, 197–204.
[9] Bjarnason, J.B. and Fox, J.W. (1995) Snake venom metalloendopeptidases: reprolysins. Meth. Enzymol. 248, 345–368.
[10] Fox, J.W. and Serrano, S.M. (2005) Structural considerations of the snake venom metalloproteinases, key members of the M12 reprolysin family of metalloproteinases. Toxicon 45, 969–985.
[11] Araki, S., Masuda, S., Maeda, H., Ying, M.J. and Hayashi, H. (2002) Involvement of specific integrins in apoptosis induced by vascular apoptosis-inducing protein 1. Toxicon 40, 535–542.
[12] Maruyama, J., Hayashi, H., Miao, J., Sawada, H. and Araki, S. (2005) Severe cell fragmentation in the endothelial cell apoptosis induced by snake apoptosis toxin VAP1 is an apoptotic characteristic controlled by caspases. Toxicon 46, 1–6.
[13] Seals, D.F. and Courtneidge, S.A. (2003) The ADAMs family of metalloproteases: multidomain proteins with multiple functions. Genes Dev. 17, 7–30.
[14] White, J.M. (2003) ADAMs: modulators of cell–cell and cell–matrix interactions. Curr. Opin. Cell. Biol. 15, 598–606.
[15] Gomis-Ruth, F.X., Kress, L.F. and Bode, W. (1993) First structure of a snake venom metalloproteinase: a prototype for matrix metalloproteinases/collagenases. EMBO J. 12, 4151–4157.
[16] Maskos, K. et al. (1998) Crystal structure of the catalytic domain of human tumor necrosis factor-alpha-converting enzyme. Proc. Natl. Acad. Sci. USA 95, 3408–3412.
[17] Orth, P. et al. (2004) Crystal structure of the catalytic domain of human ADAM33. J. Mol. Biol. 335, 129–137.
[18] Janes, P.W. et al. (2005) Adam meets Eph: an ADAM substrate recognition module acts as a molecular switch for ephrin cleavage in trans. Cell 123, 291–304.
[19] Takeda, S., Igarashi, T., Mori, H. and Araki, S. (2006) Crystal structures of VAP1 reveal ADAMs' MDC domain architecture and its unique C-shaped scaffold. EMBO J. 25, 2388–2396.
[20] Zhou, Q., Smith, J.B. and Grossman, M.H. (1995) Molecular cloning and expression of catrocollastatin, a snake-venom protein from *Crotalus atrox* (western diamondback rattlesnake) which inhibits platelet adhesion to collagen. Biochem. J. 307 (Pt 2), 411–417.
[21] Igarashi, T., Oishi, Y., Araki, S., Mori, H. and Takeda, S. (2006) Crystallization and preliminary X-ray crystallographic analysis of two vascular apoptosis-inducing proteins (VAPs) from *Crotalus atrox* venom. Acta Crystallogr. Sect. F Struct. Biol. Cryst. Commun. 62, 688–691.
[22] Otwinoski, Z. and Minor, W. (1997) in: Methods in Enzymology (Carter, C.W. and Sweet, R.M., Eds.), vol. 276, pp. 307-325.
[23] CCP4. (1994) The CCP4 suite: programs for protein crystallography. Acta Crystallogr. D Biol. Crystallogr. 50, 760–763.
[24] Roussel, A. and Cambillau, C. (1996) AFMB-CNRS, Marseille, France.
[25] Brunger, A.T. et al. (1998) Crystallography & NMR system: a new software suite for macromolecular structure determination. Acta Crystallogr. D Biol. Crystallogr. 54 (Pt 5), 905–921.
[26] Kraulis, P.J. (1991) MOLSCRIPT: a program to produce both detailed and schimatic plots of protein structure. Acta Crystallogr. D Biol. Crystallogr. 24, 946–950.
[27] Merritt, E.A.A.B. and David, J. (1997) in: Methods in Enzymology, vol. 277, pp. 505–524.
[28] DeLano, W.L. (2002) DeLano Scientific, San Carlos, CA, USA.
[29] Masuda, S., Maeda, H., Miao, J.Y., Hayashi, H. and Araki, S.-C. (2007) cDNA cloning and some additional peptide characterization of a single-chain vascular apoptosis-inducing protein, VAP2. Endothelium 14, 1–8.
[30] Bode, W., Gomis-Ruth, F.X. and Stockler, W. (1993) Astacins, serralysins, snake venom and matrix metalloproteinases exhibit identical zinc-binding environments (HEXXHXXGXXH and Met-turn) and topologies and should be grouped into a common family, the 'metzincins'. FEBS Lett. 331, 134–140.
[31] Gomis-Ruth, F.X. (2003) Structural aspects of the metzincin clan of metalloendopeptidases. Mol. Biotechnol. 24, 157–202.
[32] Kini, R.M. and Evans, H.J. (1992) Structural domains in venom proteins: evidence that metalloproteinases and non-enzymatic platelet aggregation inhibitors (disintegrins) from snake venoms are derived by proteolysis from a common precursor. Toxicon 30, 265–293.
[33] Calvete, J.J., Marcinkiewicz, C., Monleon, D., Esteve, V., Celda, B., Juarez, P. and Sanz, L. (2005) Snake venom disintegrins: evolution of structure and function. Toxicon 45, 1063–1074.
[34] Takeya, H., Nishida, S., Nishino, N., Makinose, Y., Omori-Satoh, T., Nikai, T., Sugihara, H. and Iwanaga, S. (1993) Primary structures of platelet aggregation inhibitors (disintegrins) autoproteolytically released from snake venom hemorrhagic metalloproteinases and new fluorogenic peptide substrates for these enzymes. J. Biochem. (Tokyo) 113, 473–483.
[35] Fox, J.W. and Bjarnason, J.B. (1995) Atrolysins: metalloproteinases from *Crotalus atrox* venom. Meth. Enzymol. 248, 368–387.
[36] Blobel, C.P., Myles, D.G., Primakoff, P. and White, J.M. (1990) Proteolytic processing of a protein involved in sperm-egg fusion correlates with acquisition of fertilization competence. J. Cell Biol. 111, 69–78.
[37] Blobel, C.P., Wolfsberg, T.G., Turck, C.W., Myles, D.G., Primakoff, P. and White, J.M. (1992) A potential fusion peptide and an integrin ligand domain in a protein active in sperm-egg fusion. Nature 356, 248–252.